AIAA-99-1217

Transonic Aeroelastic Analysis of a High Speed Transport Wind Tunnel Model

Myles L. Baker*
Raul Mendoza†
Peter M. Hartwich††

The Boeing Company, Phantom Works
2401 E. Wardlow Road
Long Beach, CA 90807

As part of the NASA High Speed Research (HSR) Program, a series of aeroelastic wind tunnel models were built and tested in the NASA Langley Research Center (LaRC) Transonic Dynamics Tunnel (TDT). The purpose of these wind tunnel models was to provide experimental validation that state of the art aeroelastic analysis techniques can predict the aeroelastic behavior of these configurations. As had been noted in previous high speed transport programs, aeroelasticity can have a major impact on the viability of a high speed transport, requiring large weight penalties to provide sufficient flutter margins. In this paper, one such wind tunnel model (the Flexible Semispan Model or FSM) and the corresponding analytical correlations are discussed. The flutter behavior of this model is very complex, involving large transonic effects. While linear analyses failed to accurately predict the flutter boundaries, nonlinear (Euler) flutter solutions performed in the aeroelastic Euler/Navier-Stokes solver CFL3D-AE.BA gave good correlation with experimental flutter results.

Introduction

While the interaction between aerodynamic and structural phenomena have been understood for many years, most progress in accurately predicting aeroelastic interactions has been made in flight regimes where both the aerodynamics and the structure can be modeled as linear systems. It is now common practice in the aircraft industry to compute static aeroelastic effects as well as flutter behavior for complex configurations using software packages that model the structural dynamics using a linear finite element formulation[1], and that predict the aerodynamic forces using a linear aerodynamic theory such as the Doublet-Lattice Method[2].

While these linear analysis methods have proven to be invaluable in predicting and solving aeroelastic problems, their limitations are widely recognized. In particular, it is well known that aeroelastic analysis methods based on linear aerodynamic theories do not give accurate results when applied in the transonic regime, where significant nonlinearities are present. However, with the increasing availability of high-power, low cost computing, it is rapidly becoming feasible to perform aeroelastic analyses using aerodynamics based on Computational Fluid Dynamics (CFD), which can accurately model many types of flow nonlinearities, including transonic shocks.

One of the premier CFD flow solvers currently in use is CFL3D[3,4,5], which has been developed by NASA for several years, and has been shown to accurately predict steady and unsteady aerodynamic forces in the

* Senior Engineer/Scientist, Loads and Dynamics. Member AIAA
† Engineer/Scientist, High Speed Aerodynamics.
†† Associate Technical Fellow, High Speed Aerodynamics. Associate Fellow AIAA.

presence of flow nonlinearities. This code can model the aerodynamics using either the Euler or the Navier-Stokes equations, and has recently been modified to include a robust multiblock grid perturbation algorithm[6] as well as a structural dynamic model using modal degrees of freedom similar to that used in CAP-TSD[7]. The resulting aeroelastic code is CFL3D-AE.BA, which has been in use for several years in performing nonlinear aeroelastic analyses on various configurations.

In this paper, aeroelastic analyses are performed on a generic high speed transport configuration using linear aeroelastic methods as well as CFL3D.AE-BA. The configuration analyzed is an aeroelastically scaled wind tunnel model known as the Flexible Semispan Model (FSM)[8,9]. This model was also tested in the NASA Langley Research Center (LaRC) Transonic Dynamics Tunnel (TDT), and comparisons are made between the analysis results and the experimental data. It will be shown that the nonlinear analysis performed in CFL3D-AE.BA using an aerodynamic model based on the Euler equations gives significantly better correlation with the wind tunnel results than the linear analysis.

Model Description

The FSM wind tunnel model consists of a dynamically scaled wing with a typical supersonic transport planform, which is attached to a rigid fuselage beam. Since the primary purpose of this model was to obtain data suitable for analysis/test correlation, rather than to provide a flutter clearance, the model was not intended to rigorously replicate any given airplane configuration. The airfoil section and mass/stiffness properties of the wing are loosely based on an early High Speed Civil Transport (HSCT) design, suitably modified to obtain the desired flutter mechanism in the tunnel operating envelope. The wing had two trailing-edge control surfaces and was heavily instrumented with accelerometers, strain gages, and unsteady pressure transducers. The planform and instrumentation layout of the FSM are shown in Figure 1.

There were several other ways in which the FSM was unrepresentative of a viable high speed transport. Specifically, the wing was mounted at the root to a rigid fixture, preventing the chordwise bending motion that is often dominant in a high speed transport due to the extremely long root chord and thin fuselage sections typical of such configurations. The layups used in the fiberglass skin were therefore not directly scaled from airplane skin gages, but were determined such that an HSCT-like flutter mechanism was obtained. While the flutter mechanisms presented here are not directly representative of current HSCT configurations, they show very complex interactions, and are extremely valuable from an analysis validation point of view.

During wind tunnel testing, two strongly divergent flutter points were encountered in the transonic regime, as well as a "chimney" of high dynamic response or weakly divergent "soft" flutter. This "soft" flutter occurred over a large range of dynamic pressures between Mach 0.98 and 1.00. The frequency content of the "hard" flutter points at higher dynamic pressure and the "soft" flutter points at lower dynamic pressure was different, showing that there were two distinct flutter mechanisms involved.

Finite Element Model (FEM)

The analytical structural dynamic model was a finite element model in MSC/NASTRAN[1]. The model consisted of 360 shell elements (representing the wing skins, leading and trailing edge fairings, wingtip cap, and flap skins), 146 solid elements (representing the wing core), and 66 beam and spring elements (representing the fuselage beam and backup structure). A planform view of the FEM is shown in Figure 2. The finite element model was correlated to match static and vibration test results of the wing and backup structure. In the correlation process, the mass was held constant, and the stiffness of the skin elements was modified to improve correlation. It was found that the static stiffness test results were extremely valuable in improving the analytical model because a very robust static stiffness test program had been performed, and a large amount of high-quality data was available. In the correlation process using the static stiffness test data, the finite element model was loaded at the same 12 points as the physical wing, and the resulting deflections were measured at the FEM nodes corresponding to the dial gages used in the deflection test. The vector norm of the error between the analysis and test data for all 12 load cases was then used as an objective function, and an optimization was performed to reduce this error. Skin ply thicknesses were used as design variables. The skin plies were allowed to vary by up to +/- 20%, and the error was significantly reduced for all 12 load cases. A representative wing static correlation result is shown in Figure 3 for the pre-correlation and post-correlation models.

This statically correlated FEM was then used in a vibration analysis and the frequencies and mode shapes were correlated with the modal characteristics of the physical model as measured in a ground vibration test (GVT). It was found that with the FEM tuned to match the static stiffness test results, the three most relevant mode shapes correlated very well with the GVT data, and no additional tuning to match the frequencies and mode shapes was warranted. A comparison between the GVT and analysis vibration results is shown in Figure 4. The three modes shown were chosen based on their degree of participation in the analytical flutter mechanisms.

Doublet Lattice Model

A linear aerodynamic model was constructed in order to perform linear static aeroelastic and flutter analyses. The doublet lattice model used in these

analyses is shown in Figure 2. The wing has 360 boxes (24 of which are on the trailing edge control surface). Since the fuselage is not aeroelastically active (i.e. rigid), it is not directly modeled in the doublet lattice model. Instead, the correct symmetry plane boundary condition and carry-through lift are approximated by simply extending the wing planform to the tunnel sidewall. The first three strips of the doublet lattice model represent the fuselage. No attempt to model tunnel wall interference (through reflection planes, etc.) was made.

Linear aeroelastic analyses were performed by coupling the doublet lattice model with the structural FEM. For static aeroelasticity, a direct stiffness approach was used (MSC/NASTRAN solution 144[1]), and for flutter, a p-k flutter solution was computed using the first ten vibration modes (MSC/NASTRAN solution 145[1]).

CFL3D Model

The nonlinear aeroelastic analysis was performed in CFL3D-AE.BA. The primary nonlinear flutter analysis was performed in the Euler mode, but a few points (not discussed in this paper) were analyzed with the Navier-Stokes equations. The Euler grid, shown in Figure 5, is a single block (241x65x49) grid with C-O topology. The structural dynamics are accounted for in CFL3D through the use of vibration modes. The vibration modes are identical to those used in the linear analysis, but are splined to the CFD surface grid as a preprocessing step. As in the linear analysis, the first ten vibration modes were used.

Analysis Process

A flowchart of the analysis process used in this study is shown in Figure 6. This flowchart includes the process for linear and nonlinear static and flutter analysis and the correlation with experimental data. For the static aeroelastic and flutter analysis, the structural FEM and the linear aerodynamic model are simply combined in the commercially available MSC/NASTRAN package for linear aeroelastic analysis. This process is described in detail in Reference 1.

For the nonlinear analysis, the process is somewhat more complex. The core nonlinear aeroelastic code is CFL3D.AE-BA, which includes a structural dynamic model based on modal degrees of freedom. The structural mode shapes are obtained from a code such as MSC/NASTRAN, and are interpolated to the CFD surface mesh using a spline process. This allows the coupled aeroelastic analysis including nonlinear flow phenomena to be efficiently and accurately calculated so long as the structure behavior is linear.

The first step in the nonlinear analysis process is to obtain the steady, rigid flow solution. For this step, the structural degrees of freedom are not included in the problem. This solution is then used as a starting point for the static aeroelastic solution, which is performed in order to ensure that the mean steady flow about which flutter solutions are performed is correct. The flutter solution is then initiated by computing the impulse response of the aeroelastic system about the static aeroelastic equilibrium position. This is accomplished by applying an initial velocity to the modal degrees of freedom. In all the CFL3D-AE.BA analyses shown, studies were performed on grid resolution, time step size, and number of subiterations in order to ensure that the numerical accuracy of the solution was adequate.

One of the difficulties with time-domain aeroelastic analysis is the interpretation of the resulting flutter time histories. The most common method for determining flutter boundaries from aeroelastic CFD time histories is to perform a series of analyses at different dynamic pressures. The frequencies and damping ratios at each dynamic pressure are then determined by fitting a series of damped sinusoids to the resulting time history data. So long as the range of dynamic pressures considered brackets the flutter crossing, the crossing can be identified by interpolating damping values between the dynamic pressures. While this process has been successful in previous studies, it has shortcomings when the complexity of the case is increased. For cases with large numbers of structural modes, the fitting of the series of damped sinusoids to the time history data can be cumbersome, labor-intensive, and error-prone. An improved process has been developed in the SYSID code, in which an equivalent linear state-space model is identified that replicates the aeroelastic response of the system. The eigenvalues of this identified model then give the frequency and damping information of interest. This process allows monitoring of the estimated eigenvalues as the simulation progresses in order to ensure that the time history is long enough to obtain converged eigenvalue estimates, and through interpolation on the resulting state-space models, trends of frequency and damping with changes in dynamic pressure can be approximated.

Results

Static Aeroelasticity

A necessary step in obtaining the correct flutter behavior is to obtain the correct static aeroelastic solution. An extensive set of static aeroelastic analyses of the FSM was performed, using linear Doublet-Lattice aerodynamics as well as the nonlinear CFL3D.AE-BA Euler analysis. As part of this correlation effort, the detailed pressure distributions from the analyses were compared with the steady and unsteady pressure distributions from the unsteady pressure transducers, and the overall lift, pitching, and rolling moments on the wing were correlated with the analysis. A representative result is shown in Figure 7. This figure shows the variation in the normalized lift curve slope of the wing for various Mach numbers. The test data is shown, as

well as the results of a linear aeroelastic computation using Doublet-Lattice (subsonic) or ZONA[10] (supersonic) aerodynamics in MSC/NASTRAN, as well as the static aeroelastic solution from CFL3D-AE.BA. The improvement of the Euler aeroelastic solution from CFL3D over the linear analysis is clearly seen, especially in the transonic regime. As expected, the linear analysis performs very well in the subsonic regime. Similar results were seen for pitching and rolling moments. It should be noted that there is still some discrepancy between the aeroelastic Euler solutions and the test data. It is expected that this discrepancy will be reduced by including the effects of viscosity using the Navier-Stokes equations.

Linear Flutter Analysis

The results of a linear flutter analysis are shown in Figures 8 and 9. Figure 8 shows a typical flutter result at a single Mach number without the effects of structural damping. The left hand portion of Figure 8 shows variation in the aeroelastic modal frequencies with changes in dynamic pressure, while the right hand portion shows variation in damping (positive damping denotes an instability). Note that in the range of interest of dynamic pressure, there are two distinct flutter mechanisms. The lower frequency mechanism is a "hump" mode with a frequency approximately 1.66 times the first modal frequency. The higher frequency mechanism is a "hard" flutter crossing with a frequency approximately 1.9 times the first modal frequency.

When similar results for all Mach numbers considered are combined along with the effects of structural damping, the flutter stability boundaries shown in Figure 9 result. Note that the zone of instability predicted by the linear theory for the "hump" mode covers a relatively wide Mach and dynamic pressure range. The "hard" flutter crossing shows an instability boundary that varies slowly with changes in Mach number.

Results of the flutter experiment are also shown in Figure 9. The open circles show points where divergent or high amplitude oscillations were encountered in the flutter test. Note that the experimental flutter points are concentrated in a very narrow Mach range in the high transonic regime, and cover a large range of dynamic pressures. This results in a chimney-shaped flutter boundary as shown in Figure 9. At lower Mach numbers, the flutter dynamic pressure is significantly higher, correlating fairly well with the linear "hard" flutter boundary.

Flutter mechanisms that show the "hump" behavior illustrated in Figure 8 are very sensitive to small changes in structural and aerodynamic modeling, and are very difficult to predict analytically. The conjecture (which will be validated in the following sections) is that the "hump" mode is, in reality, slightly stable in general, but that transonic interactions near Mach 1.0 cause a decrease in damping. This destabilizes the hump mode over a large range of dynamic pressures between Mach 0.98 and 1.0, resulting in the "chimney" seen in the experimental flutter boundary. The experimental instabilities near dynamic pressures of $0.85Q_0$ are of higher frequency, and are related to the "hard" flutter crossing shown in Figure 8.

Nonlinear Flutter Analysis

A series of nonlinear flutter analyses were performed ranging from Mach 0.8 to Mach 1.02, and dynamic pressures from $0.5Q_0$ to Q_0. Two representative results are shown in Figures 10 and 11. Figure 10 shows a result for a CFD simulation at Mach 0.80. At this Mach number, the flow (and hence the aeroelastic behavior) is fairly linear, and the results are nicely behaved. The output of the CFL3D.AE-BA code is shown in Figure 10(a). This is simply the time history data of the generalized (modal) deflections. The simulation was performed with 10 modes, and two are shown here as an illustration. It is clear from these plots that nothing is clear from these plots. The aeroelastic interactions for this configuration are complex, resulting in a large degree of coupling in the modal time histories, and the resulting interactions make it extremely difficult to determine stability or instability "by eye." However, it can be said that there is no obvious exponential growth (instability) in the time histories.

A more quantitative determination of the stability/instability of this condition is shown in Figure 10(b). This shows the estimated aeroelastic frequencies and dampings identified from the time history data as a function of iteration number. Note that it takes approximately 100 iterations of the CFD simulation to provide a sufficient amount of data for reliable eigenvalue estimates. Good convergence of the eigenvalues is obtained after approximately 250 iterations. The results indicate that there is a slight instability at a frequency of approximately $1.65f_0$, but the unstable aerodynamic damping is so small that it will be stabilized through structural damping. These eigenvalue estimates from the SYSID code have proven to be an automated and robust method for determining flutter stability or instability from a CFD time history.

Figure 10(c) shows an estimate of the trends in frequency and damping with changes in dynamic pressure. This plot is constructed by interpolating between the identified state-space models at different dynamic pressures. The frequencies and dampings from such a plot are not exact (except at the points where CFD solutions are run), but provide useful information to the aeroelastician as to the aeroelastic interactions that are occurring. In this case, it is encouraging to compare these Q-g and Q-f plots to the linear results and note that the aeroelastic mechanisms identified are identical. There is clearly a "hump" mechanism at lower frequency and lower dynamic pressure, and a "hard" flutter crossing at a higher frequency and dynamic pressure, similar to those mechanisms seen in Figure 8.

Figure 11 shows similar results for a more challenging case. These plots are for a truly transonic case at Mach 0.98 and dynamic pressure of $0.67Q_0$. In this case, it is clear from the time history that this simulation is unstable, since exponential growth can be seen in the modal response. The corresponding eigenvalue estimates are shown in Figure 11(b). Again, after approximately 250 iterations, the eigenvalue estimates are fairly well converged. Since this case is truly transonic and includes significant nonlinear dynamics induced by shock motion, the linear state space model will never completely converge. Indeed, small oscillations in the damping estimates in Figure 11(b) are observed to the end of the simulation. The unstable mechanism is approximately $1.65f_0$, consistent with the "hump" mode predicted by the linear theory and the experimental "chimney" results.

In the nonlinear case shown, the state-space models identified at different dynamic pressures were not sufficiently similar to allow meaningful interpolation and construction of approximate Q-g and Q-f plots. In this case, the flutter crossing was estimated by interpolating between solutions to find the zero damping point.

The nonlinear flutter results are summarized in Figure 12. In this plot, all CFD simulations are shown, and the symbol is a square if the simulation showed no instabilities, and a triangle if an instability was found. The resulting flutter stability boundary is also plotted. Excellent correlation of flutter boundaries and frequency of instabilities between the analysis and the experimental results was obtained.

Concluding Remarks

Transonic flutter analyses have been performed on a dynamically scaled semispan wind tunnel model of a generic supersonic transport configuration. The analyses were performed using a linear structural dynamic model and a range of aerodynamic models ranging from linear lifting surface theory to the Euler equations. Comparison of experimental data and linear and nonlinear analytical static aeroelastic results show that the nonlinear aeroelastic solutions based on the Euler equations agree much better with the experiment than the linear analysis.

Flutter analysis of the FSM was also performed using linear and nonlinear processes, and the results were compared with the experimental flutter data. The correlation between linear analysis and the test data showed good correlation for the flutter mechanisms, but the flutter boundary was not well-predicted by the linear theory, particularly for a hump mode instability. The nonlinear flutter analysis based on the Euler equations, on the other hand, showed very good correlation with the experiment. This includes the prediction of a very narrow chimney of instability between Mach 0.98 and 1.00.

Acknowledgment

The wind tunnel model described in this paper was designed, built, and tested by the NASA LaRC Aeroelasticity Branch. Their support and assistance is greatly appreciated. Special thanks to Walt Silva, Don Keller, Stan Cole, James Florance, Vic Spain, Dave Turnock, and researchers from the Lockheed Engineering Sciences & Management Company.

References

1. Rodden, W.P. and Johnson, E.H., MSC/NASTRAN Aeroelastic Analysis User's Guide, Version 68, The MacNeal-Schwendler Corporation, 1994.
2. Albano, E., and Rodden, W.P., "A Doublet-Lattice Method for Caclulating Lift Distributions on Oscillating Surfaces in Subsonic Flows," *AIAA Journal*, Vol. 7, pp. 279-285, 1969.
3. Biedron, R.T., and Thomas, J.L., "A Generalized Patched-Grid Algorithm with Application to the F-18 Forebody with Actuated Control Strake," *Computing Systems in Engineering*, Vol, 1, No. 2-4, 1990, pp. 563-576.
4. Thomas, J.L., Krist, S.L., and Anderson, W.K., "Navier-Stokes Computation of Vortical Flows Over Low Aspect Ratio Wings," *AIAA Journal*, Vol. 28, February 1990, pp. 205-212.
5. Vasta, V.N., Thomas, J.L., and Wedan, B.W., "Navier-Stokes Computations of a Prolate Spheroid at Angle of Attack," *Journal of Aircraft*, Vol. 26, November 1989, pp. 986-993.
6. Hartwich, P.M. and Agrawal, S., "Method for Perturbing Multiblock Patched Grids in Aeroelastic and Design Optimization Applications," AIAA Paper 97-2038-CP, June 1997.
7. Cunningham, H.J., Batina, J.T., and Bennett, R.M., "Modern Wing Flutter Analysis by Computational Fluid Dynamics Methods," *Journal of Aircraft*, Vol. 25, October 1988, pp. 962-968.
8. Silva, W.A., et. al., *HSR Flexible Semispan Model Data Notebook*, unpublished, August 1996.
9. Hartwich, P.M., Baker, M.L., and Jafroudi, H., "Flexible Semispan Model (FSM) Analysis/Test Correlation," High Speed Research – Airframe Technology, Technical Milestone Report MDC CRAD-9408-TR-3342, September 1997.
10. Liu, D.D., James, D.K., Chen, P.C., and Pototzky, A.S., "Further Studies of Harmonic Gradient Method for Supersonic Aeroelastic Applications," *Journal of Aircraft*, Vol. 28, pp. 598-605..

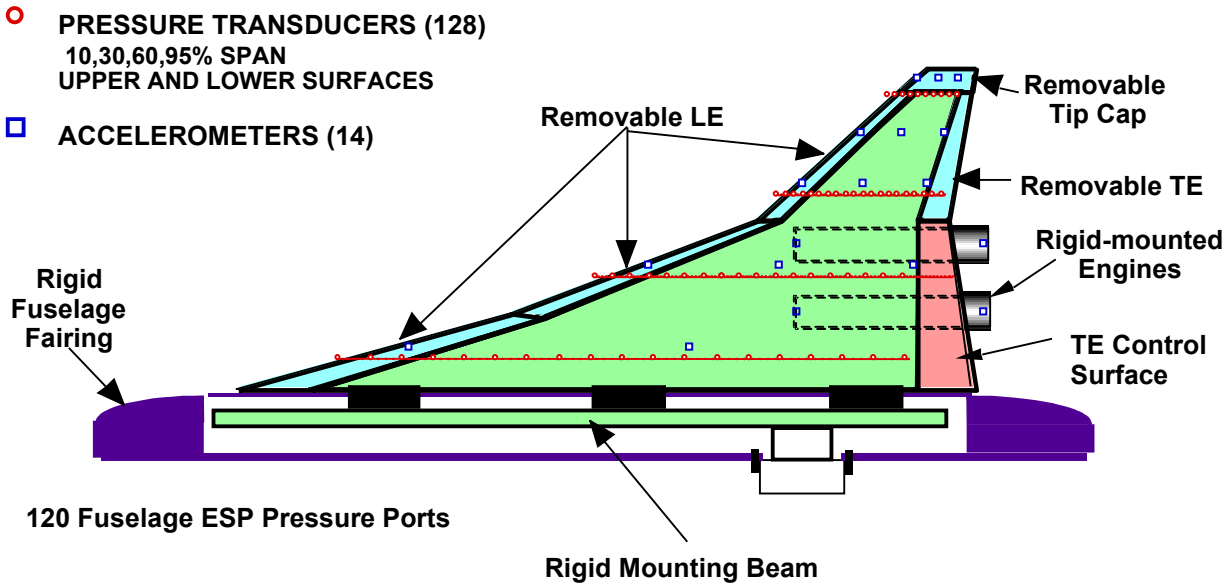

Figure 1: FSM Planform and Instrumentation Layout.

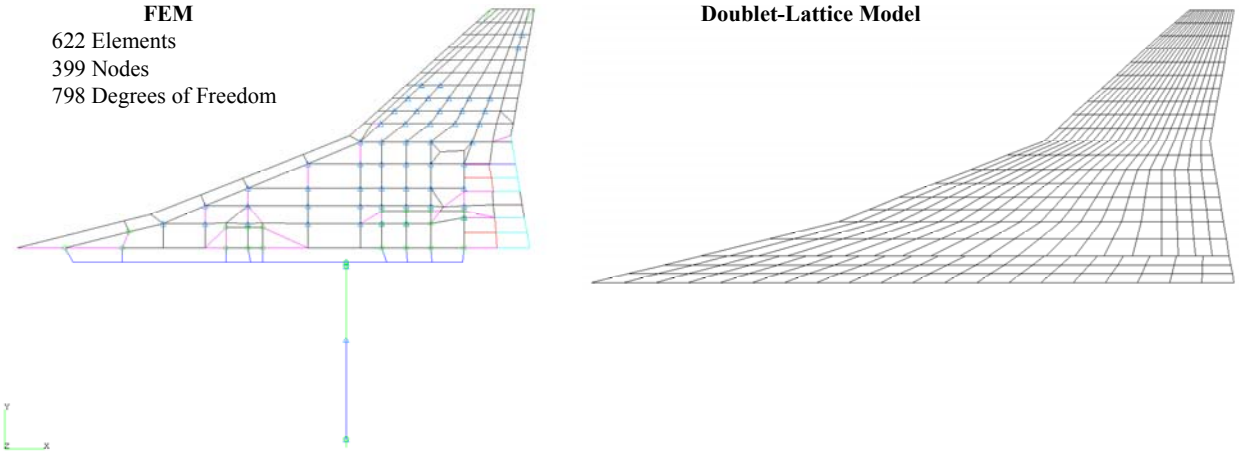

Figure 2: Finite Element and Doublet Lattice Models.

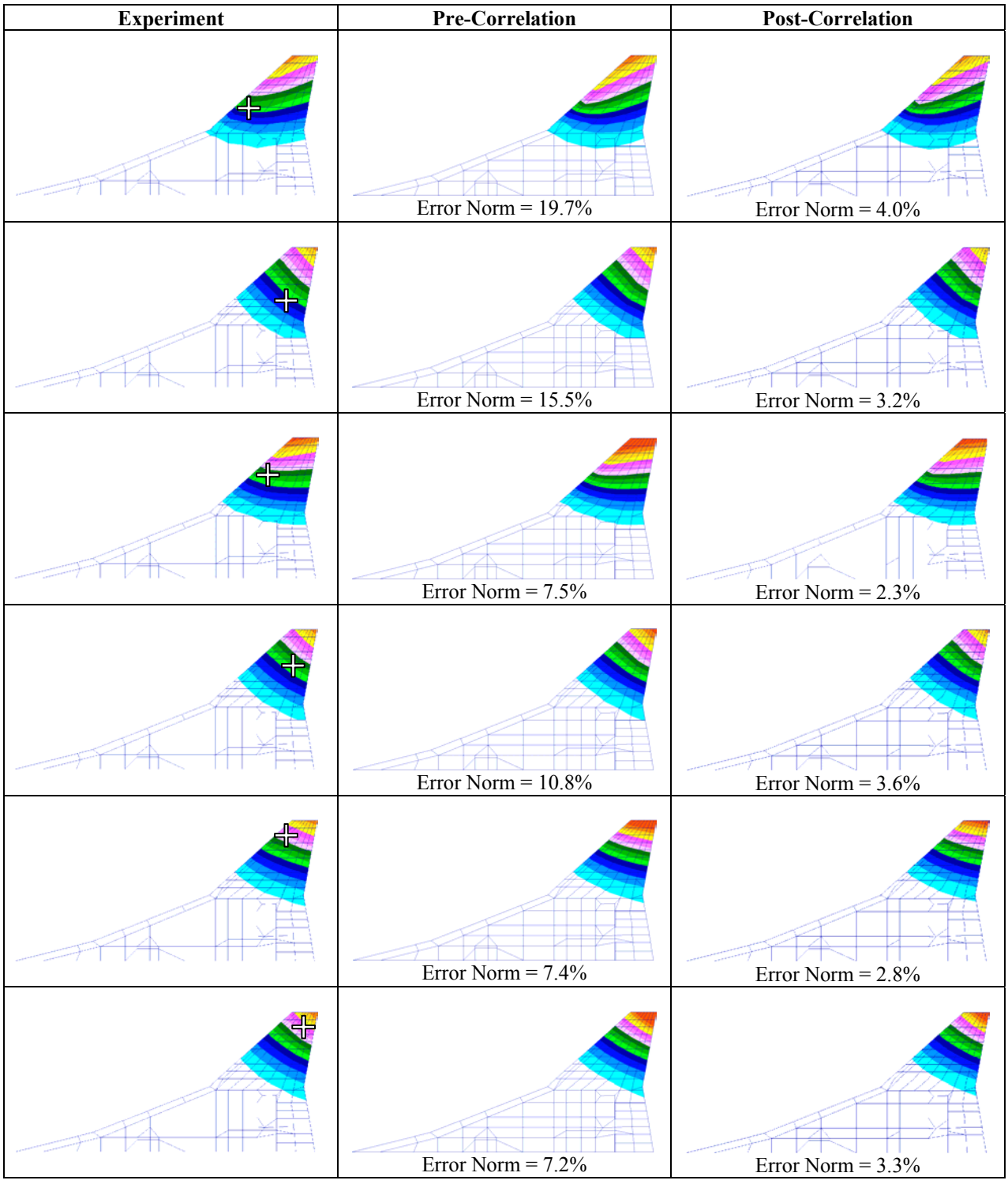

Figure 3: Static Deflection Comparison Between FEM and Test Data. Cross denotes load application point.

Mode	Test	Analysis
1	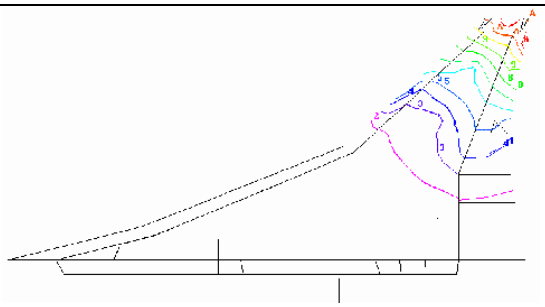 Frequency = 1.0 f_0 MCF Value = 98.9%	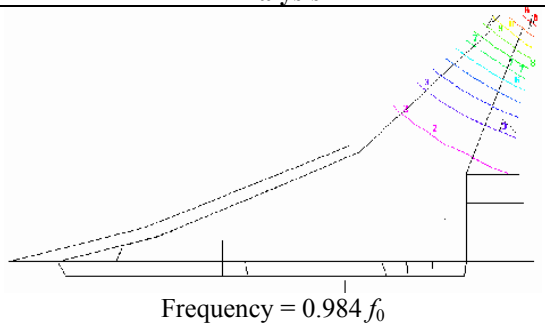 Frequency = 0.984 f_0 MAC Value = 96.8%
3	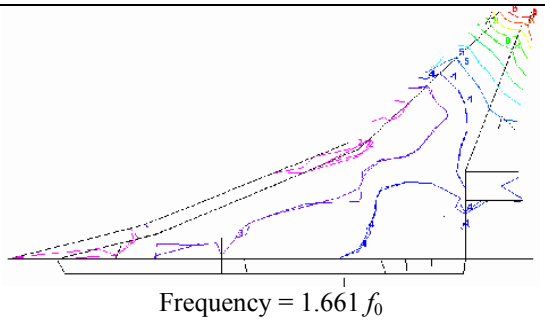 Frequency = 1.661 f_0 MCF Value = 91.6%	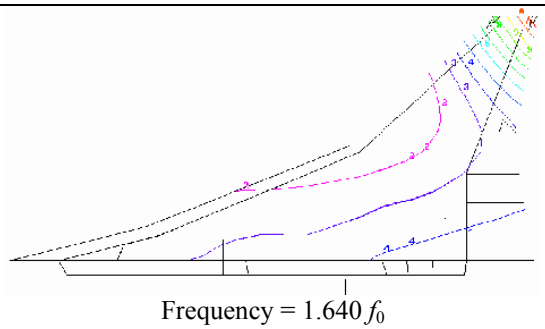 Frequency = 1.640 f_0 MAC Value = 86.9%
4	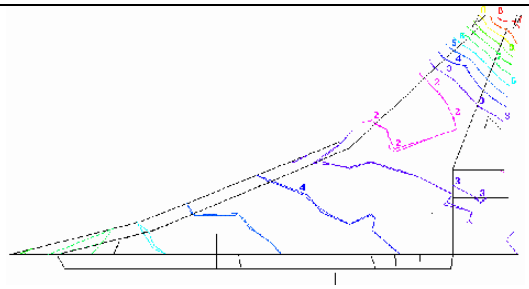 Frequency = 2.297 f_0 MCF Value = 82.3%	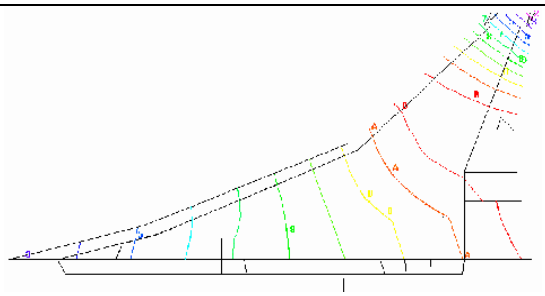 Frequency = 2.296 f_0 MAC Value = 82.8%

Figure 4: Comparison of Three Relevant Vibration Modes (FEM vs. Test Data).

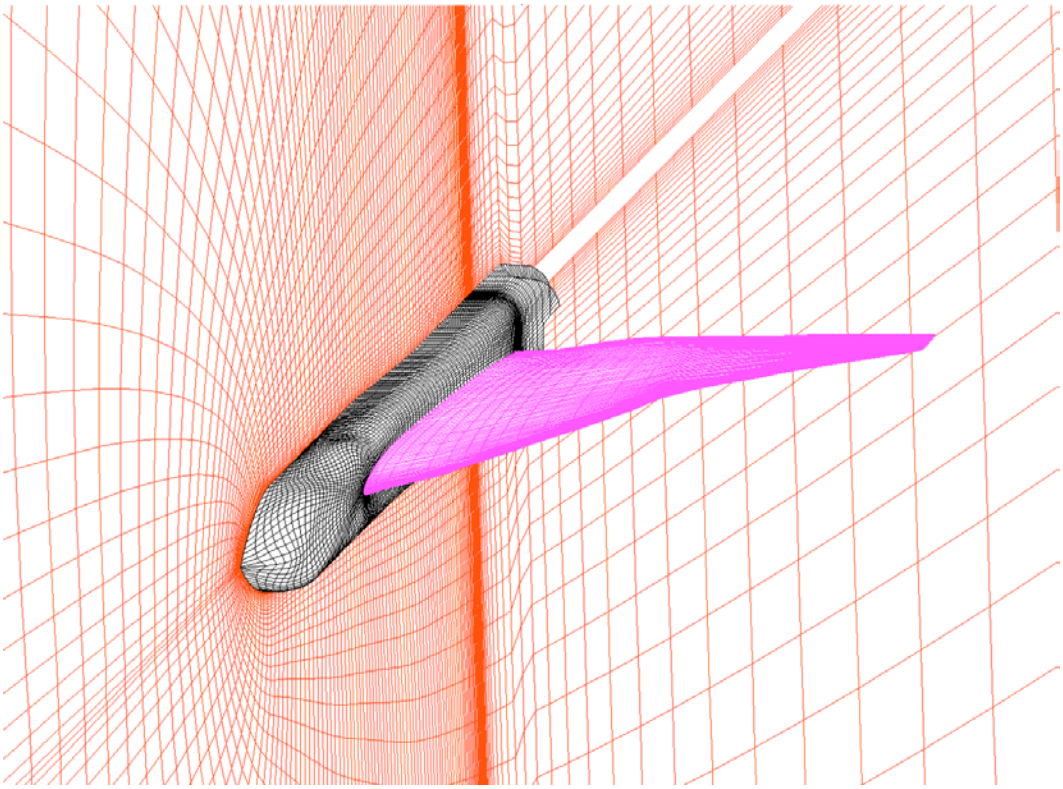

Figure 5: Euler CFL3D-AE.BA Mesh Used in Nonlinear Aeroelastic Analyses

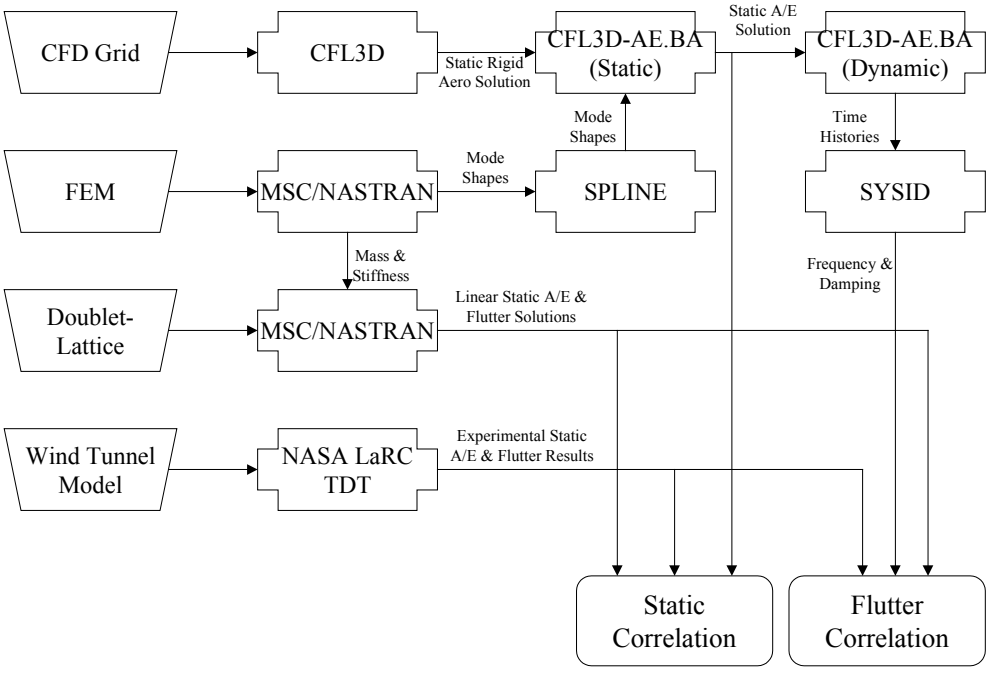

Figure 6: Flowchart of Analysis Process Used in This Study.

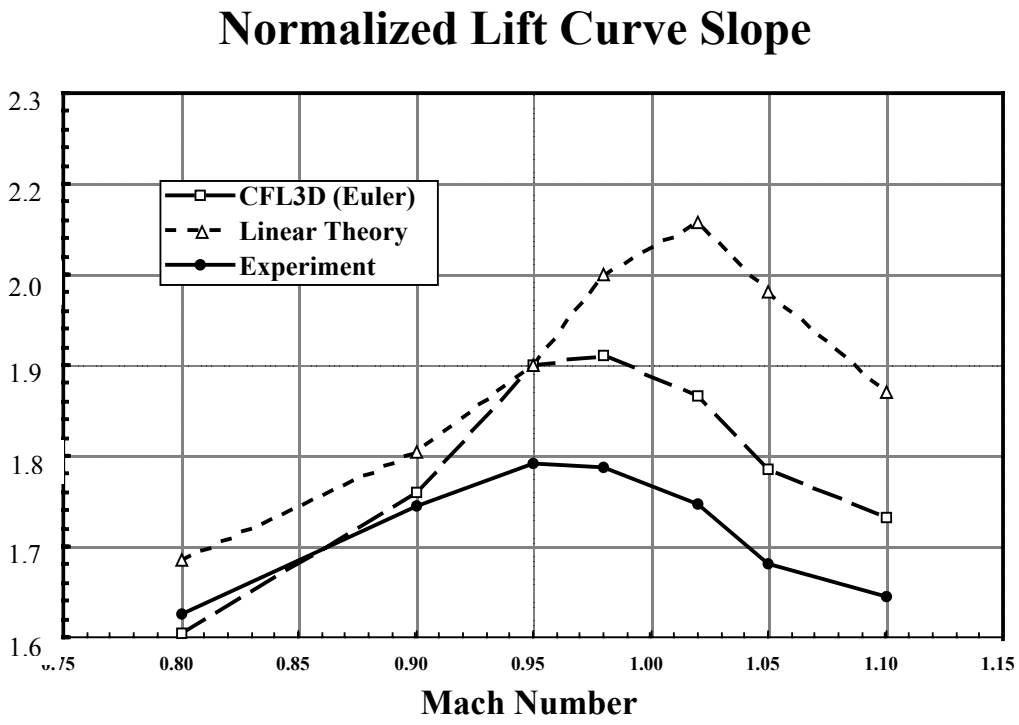

Figure 7: Normalized comparison between experimental and analytical (linear and nonlinear) aeroelastic lift curve slopes

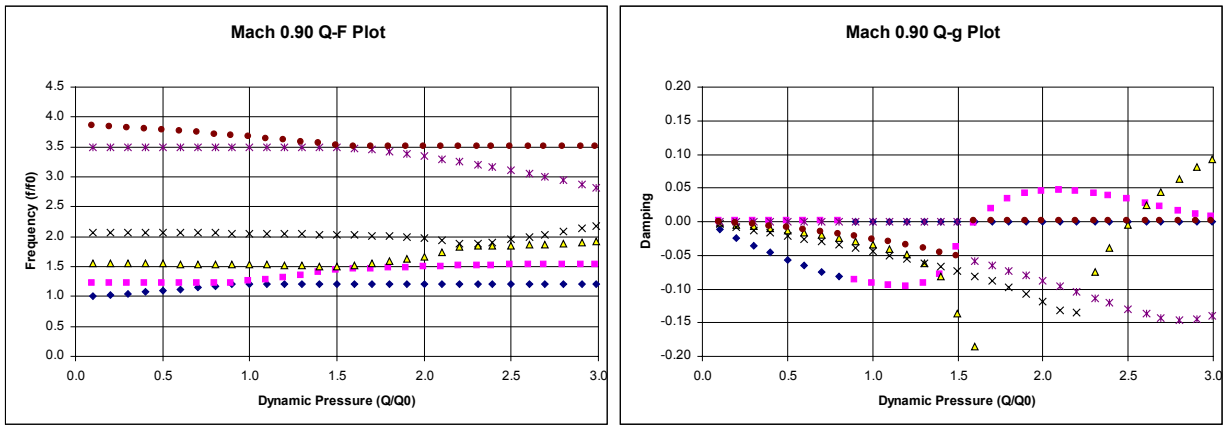

Figure 8: Typical linear flutter results. Note two significant flutter mechanisms (lower frequency "hump" mode and higher frequency "hard" mode).

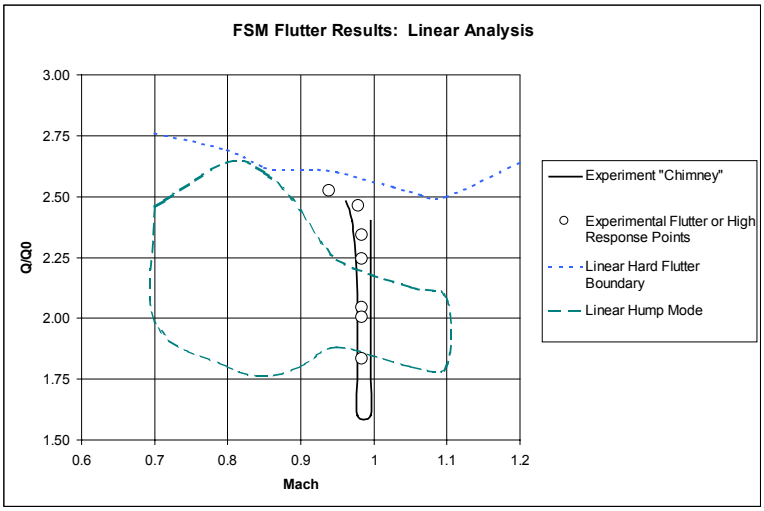

Figure 9: Flutter boundaries from linear flutter analysis and correlation with experiment.

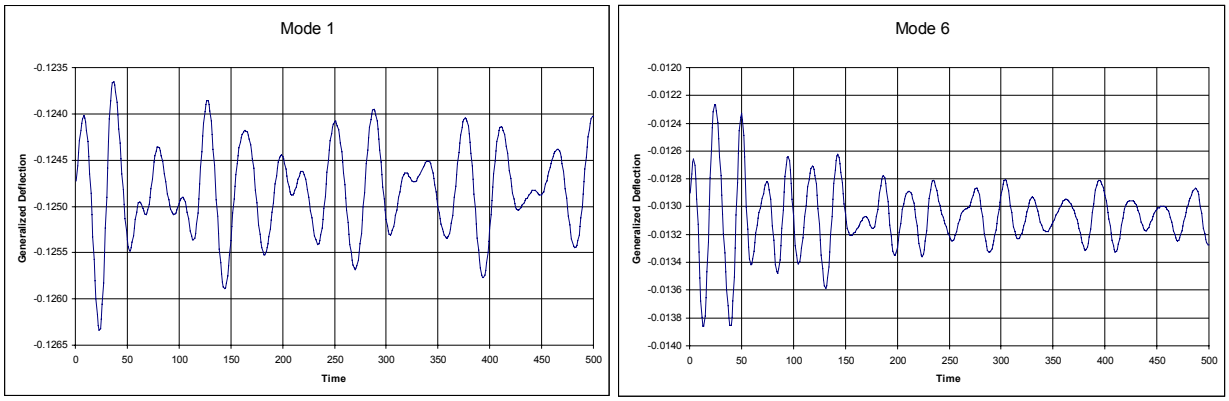

(a) Time histories of generalized (modal) deflections

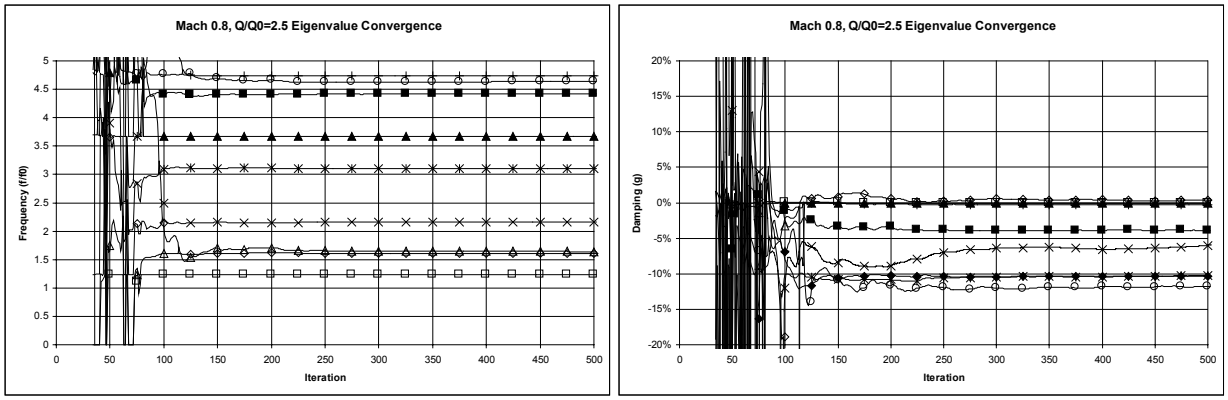

(b) Convergence of Eigenvalue Estimates from time history data

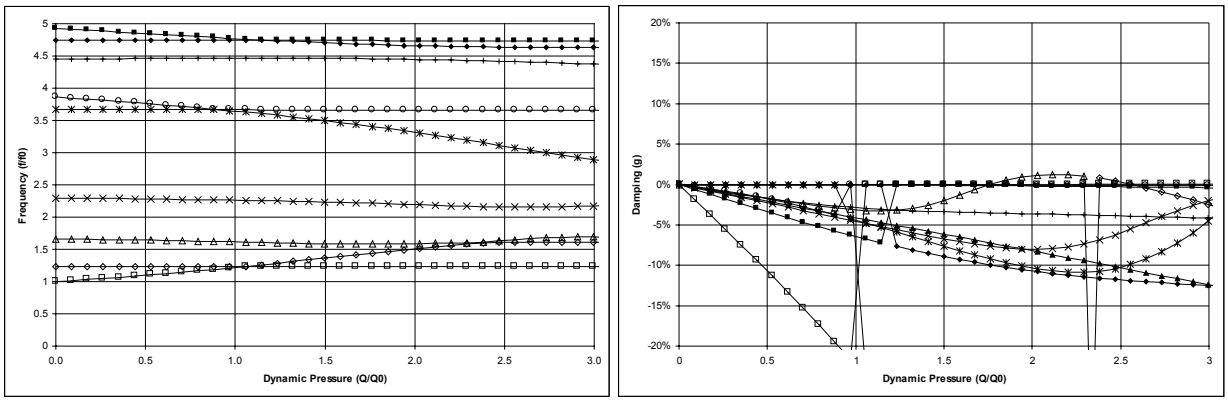

(c) Estimation of variation in frequency & damping with changes in dynamic pressure

Figure 10: Typical nonlinear flutter analysis results (Mach 0.80, Q/Q_0=2.5). Generalized deflection time histories from CFL3D.AE-BA, eigenvalue estimates from SYSID, and approximate Q-G/Q-F plots.

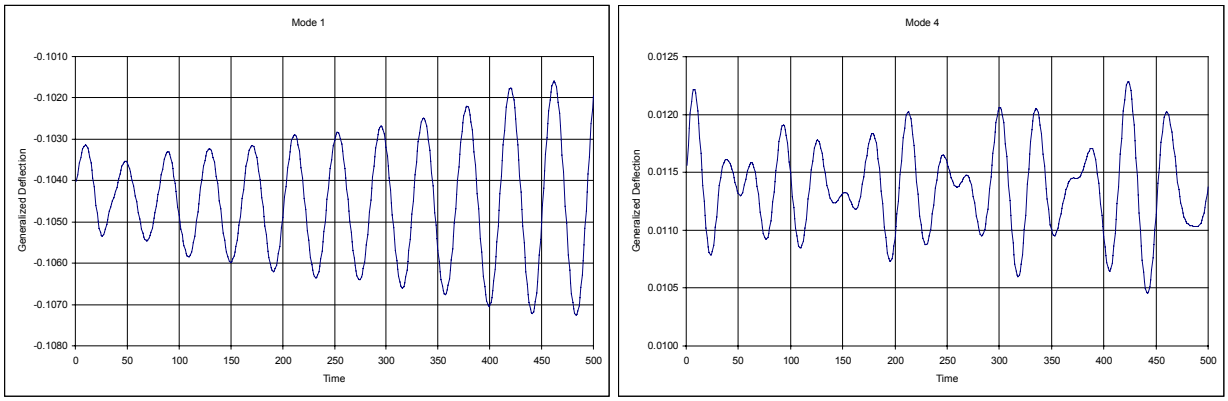

(a) Time histories of generalized (modal) deflections

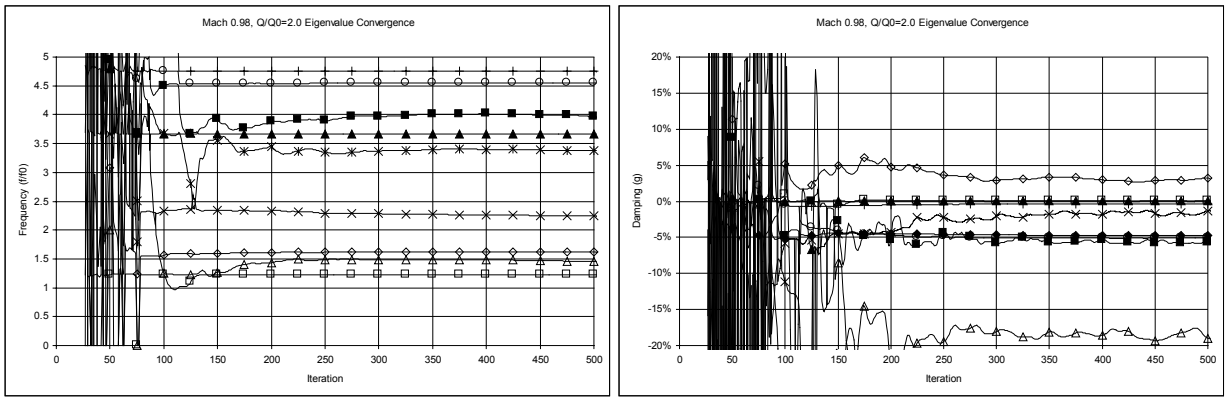

(b) Convergence of Eigenvalue Estimates from time history data

Figure 11: Typical nonlinear flutter analysis results for a tranosnic case (Mach 0.98, Q/Q_0=2.0). Generalized deflection time histories from CFL3D.AE-BA and eigenvalue estimates from SYSID.

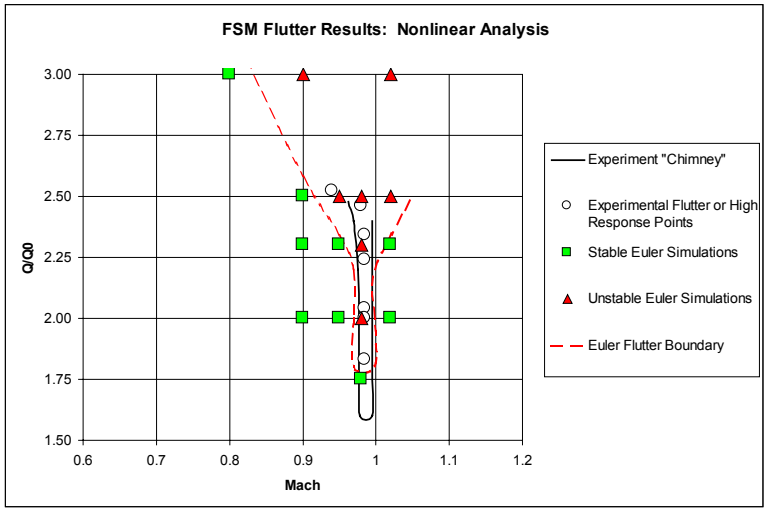

Figure 12: Flutter boundaries from nonlinear CFL3D-AE.BA flutter analysis and correlation with experiment.